Available online at www.sciencedirect.com
ScienceDirect
Journal of Photochemistry and Photobiology A: Chemistry 186 (2007) 349–356
Journal of Photochemistry and Photobiology A:Chemistry
www.elsevier.com/locate/jphotochem

Photophysical evaluation of synergism from critical micelle temperature of mixed triblock polymer micelles

Mandeep Singh Bakshi *, Navjot Kaur, Rakesh Kumar Mahajan *

Department of Chemistry, Guru Nanak Dev University, Amritsar 143005, Punjab, India

Received 9 July 2006; received in revised form 25 August 2006; accepted 1 September 2006
Available online 29 September 2006

Abstract

The critical micelle temperatures (*cmt*) of binary mixtures of triblock polymer (TBP) of poly(ethylene oxide) block poly(propylene oxide) block poly(ethylene oxide) (L64, P103, P84, P104) with different PPO/PEO ratios were determined employing the fluorescence measurements. The photophysical properties of pyrene due to its quenching as well as excimer formation in the interior of the mixed TBP micelles were studied and explained on the basis of stability of the mixed micelles. It was observed that the mixed micelle formation between the unlike components of P103 + L64 and P103 + P84 mixtures formed due to the attractive interactions and which raised from the mutual compatible arrangement among the unlike TBP monomers in the mixed state so as to minimize the steric hindrances. The results were fully supported by the viscosity measurements.

Keywords: Triblock polymers; Critical micelle temperature; Mixed micelles; Fluorescence measurements

1. Introduction

Poly(ethylene oxide) block poly(propylene oxide) block poly(ethylene oxide) (PEO–PPO–PEO) triblock polymers (TBP) are known to have micelle formation with respect to the variation of temperature. At a particular temperature where this micelle formation occurs is known as critical micelle temperature [1–8] (*cmt*), an analogous term used for this purpose to that of critical micelle concentration [4–8] (*cmc*) where micelle formation occurs due to a change in concentration. Although, most of the TBP's also show *cmc* process quite clearly, the presence of *cmt* in such polymers is relatively much clear and significant. At a particular concentration, an increase in the temperature leads to a sudden dehydration of poly(propylene oxide) (PPO) blocks which have relatively much weaker electrostatic interactions with water molecules in comparison to that of poly(ethylene oxide) (PEO). This process drags the PPO groups away from water and gathered them in the centre of an aggregate surrounded by more hydrophilic PEO groups. This leads to a conventional micelle type assembly with predominantly hydrophilic groups (PEO) arranged at the periphery while hydrophobic ones (PPO) constitute the core [1–3,9–15]. Such a transition is quite significant and occurs within a narrow temperature range.

Several techniques [5,16] have been applied to determine the *cmt* while pyrene fluorescence spectroscopy is considered to be more useful due to its much better accuracy. A much lower pyrene concentration (less than 10^{-6} M) is sufficient to detect this change which does not influence the overall micelle formation process.

Though, several studies [5,16–19] have been reported on the *cmt* for various TBP's little is known about the mixed *cmt* behavior of binary TBP mixtures. Since TBP's are categorized in the category of nonionic polymeric surfactants, therefore, ideal mixing is generally expected in the TBP–TBP mixed systems. Recently, we have observed [20] that it is not always true, and the binary mixtures of TBP's do lead to a nonideal mixing when there is a significant difference between their molecular weights or hydrophobic/hydrophilic (PPO/PEO) ratio. This actually we evaluated from the mixed *cmc* values. However, *cmt* of TBP's is considered to be having more relevance as far as their shelf life under varying temperatures is concerned. This is due to the fact that most of the industrial products in the cosmetic industry consist of more than one TBP component where a basic under-

* Corresponding authors.
E-mail address: ms_bakshi@yahoo.com (M.S. Bakshi).

1010-6030/$ – see front matter © 2006 Elsevier B.V. All rights reserved.
doi:10.1016/j.jphotochem.2006.09.004

standing on the nature of their mixed *cmt* values becomes quite important. At this end, we have selected some TBP binary mixtures on the basis of their different PPO/PEO ratios to evaluate their mixed *cmt* behavior.

2. Experimental

2.1. Materials

The TBP used in this study have the general formula $H(–OCH_2CH_2–)_n[–OCH(CH_3)CH_2–]_m(–OCH_2CH_2–)_nOH$. Table 1 lists the molecular specifications of various TBP used in the present study and all the components have been used without further purifications. Pyrene was obtained from Aldrich and was used as received. Water was purified by deionization followed by double distillation. All solutions were prepared by mass within the accuracy of ±0.01 mg. The mole fractions were accurate to ±0.0001 units.

2.2. Sample preparation

Stock solutions of different pure TBPs have been made in pure water by keeping the total concentration of each TBP = 5×10^{-4} mol dm^{-3}. The change in the concentration has drastic effect on the *cmt* of TBP. For instance, increase in the concentration leads to a large decrease in *cmt* [5]. We prefer to keep the TBP concentration constant so that concentration effect can be eliminated and only temperature effect could be studied. These stock solutions were then mixed in different proportions to make binary combinations covering whole mixing range. The mole fractions of each component of various such binary mixtures have been expressed only on the solute basis.

2.3. Methods

2.3.1. Fluorescence measurements

A constant amount of pyrene (2.0×10^{-5} mol dm^{-3}) has been maintained in all solutions. Fluorescence spectra of pyrene were obtained using Hitachi F-2500 fluorescence spectrophotometer, at an excitation wavelength of 334 nm. The intensities I_1 and I_3 were measured at the wavelengths corresponding to the first and third vibronic bands located at ca. 373 and 384 nm, while I_{exc} is measured at 470 nm. The ratios I_1/I_3 of pyrene as a function temperature were used to directly determine the *cmt*. The desired temperature was maintained by circulating the thermostated water by using Julabo F25 thermostat within the uncertainties of ±0.01 °C.

Table 1
Molecular characteristics of PEO–PPO–PEO triblock polymers

TBP	General formula	Hydrophobic/ hydrophilic ratio	MW
L64	$(EO)_{13}(PO)_{30}(EO)_{13}$	1.52	2900
P103	$(EO)_{17}(PO)_{60}(EO)_{17}$	2.32	4950
P84	$(EO)_{19}(PO)_{43}(EO)_{19}$	1.49	4200
P104	$(EO)_{18}(PO)_{58}(EO)_{18}$	2.12	5900

2.3.2. Viscosity measurements

The efflux times of binary mixtures of TBP solutions have been determined with the help of Ubbelohde type suspended level capillary viscometer sealed in a glass jacket to circulate the thermostated water at 45 °C. The efflux time was kept long to minimize the need for applying the kinetic corrections to the observed data. Each experiment was carried out after giv-

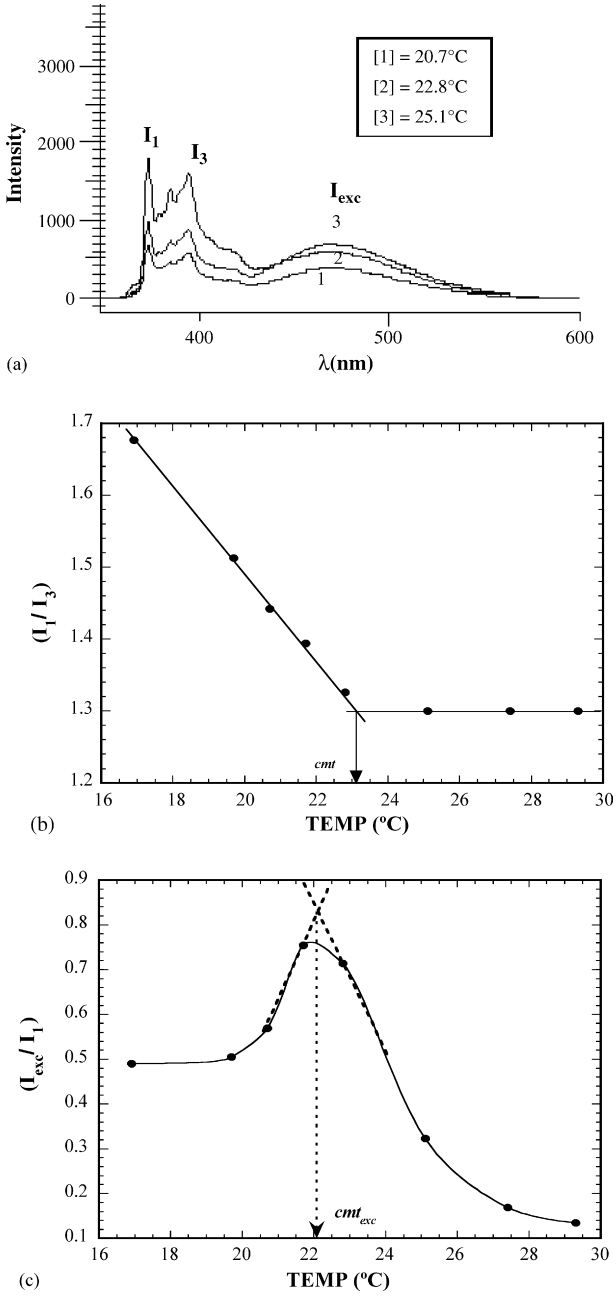

Fig. 1. (a) Pyrene emission spectrum at various temperatures of [P103] = 5×10^{-4} mol dm^{-3}: [1] 20.7 °C, [2] 22.8 °C, [3] 25.1 °C, where I_1, I_3, and I_{exc} are the intensities of first, third, and excimer bands of pyrene. (b) Variation of the pyrene intensity I_1/I_3 ratio with temperature for pure P103. (c) Variation of the pyrene intensity I_{exe}/I_1 ratio with temperature for pure P103.

ing the long-time thermal stability. Good reproducibility can be obtained by properly cleaning the viscometer with concentrated chromic acid each time before starting a set of experiments to avoid the formation of air bubbles in the viscometer. From the ratio of efflux times of the test solution, t, to that of the reference solution, t_0, i.e. water, the relative viscosity can be calculated, $\eta_r = t/t_0$, by ignoring the density corrections for the dilute solutions.

The η_r of various mole fractions of each binary mixture have been determined over the whole mixing range.

3. Results and discussion

Fig. 1(a) shows the typical pyrene emission spectrum of $[P103] = 5.0 \times 10^{-4}$ mol dm^{-3} at various temperatures. The initial five peaks represent the five vibronic bands of pyrene emission spectrum in the range of 350–420 nm, while a structure less broad band with maximum around 470 nm indicates the excimer formation. One can see that as the temperature increases the intensity ratio of I_1/I_3 band decreases whereas the intensity of excimer band increases. The former bands are due to the

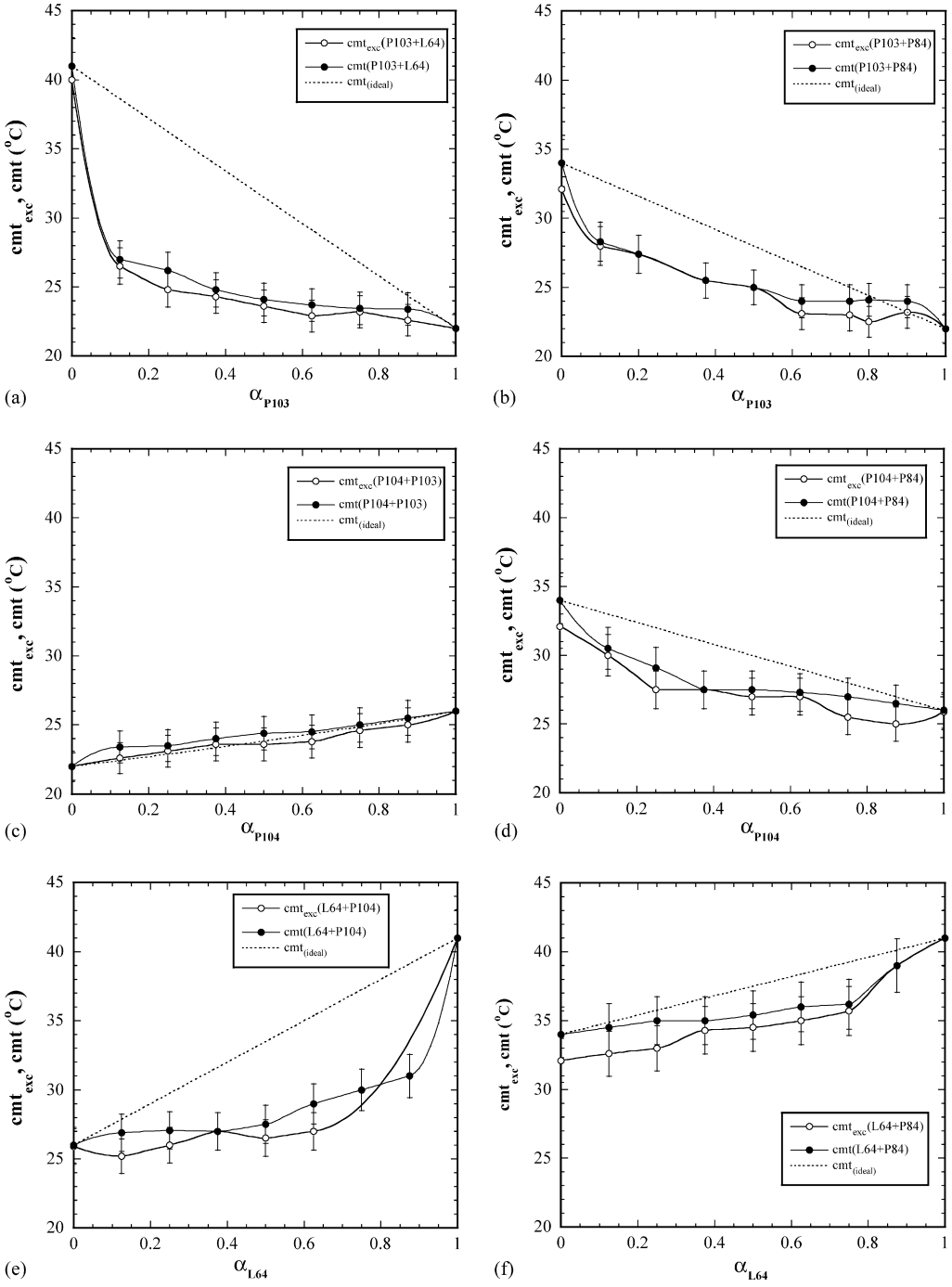

Fig. 2. Plot of cmt_{exc}, cmt (°C) vs. $\alpha_{P103,P104,L64}$: (a) P103 + L64, (b) P103 + P84, (c) P104 + P103, (d) P104 + P84, (e) L64 + P104 and (f) L64 + P84 binary mixtures.

monomeric nature of pyrene and decrease in their intensity ratio demonstrates the solubilization of pyrene monomeric species in a nonpolar environment, the strength of nonpolar environment increases with the increase in temperature. At this stage, there are more than one pyrene species in the confined hydrophobic environment and which leads to an interaction between excited and ground state pyrene species thereby resulting in the excimer formation. Such a switchover from monomer to excimer formation is clearly visible in Fig. 1(a) and is indicated by a decrease in the intensity ratio of monomer pyrene emission spectrum and increase in the intensity of excimer formation. Thus, a plot of I_1/I_3 versus temperature (Fig. 1(b)) will indicate a change in the polarity of the medium in which it is solubilized. Simultaneously, another plot of I_{exc}/I_3 (Fig. 1(c)) suggests the amount of excimer formation. One would see that I_1/I_3 value initially decreases with an increase in temperature before reaching to a constant value. At low temperature, there are no well defined micelles in the aqueous phase and pyrene predominantly remains in the aqueous phase. Further increase in the temperature sets in the micelle formation process which triggers the simultaneous solubilization of pyrene in the micelles which results in an instant fall in the I_1/I_3 ratio. The temperature where this phenomenon occurs is known as the *cmt*. Since this facilitates the solubilization of more pyrene species and thus leads to the excimer formation. The I_{exc}/I_3 plot likewise shows an instant increase which passes through a strong maximum. The temperature at which the maximum appears further corresponds to *cmt* and is represented by cmt_{exc}. The *cmt* and cmt_{exc} values thus determined (Fig. 1) have been graphically shown in Fig. 2, while the values for pure components have been listed in Table 2 and compared with literature values. Fig. 2 shows that both *cmt* and cmt_{exc} values vary nonlinearly over the whole mole fraction range when two TBP components are mixed in different proportions. The ideal behavior can be determined simply from the additivity rule when there are no interactions between the components in the mixed state and the micelles are expected to be predominantly monodisperse:

$$cmt_{(ideal)} = \alpha_1 cmt_1 + (1 - \alpha_1) cmt_2 \quad (1)$$

where cmt_1, cmt_2, and α_1, $(1 - \alpha_1)$ are the values of pure 1 and 2 components. The $cmt_{(ideal)}$ values thus calculated have also been plotted in Fig. 2 as dotted line for corresponding mixtures.

All frames of Fig. 2 show that the experimental *cmt* values for various binary mixtures mostly show negative deviations from ideality except in the case of P104 + P103 where the *cmt* values mainly lie close to that of ideal behavior. A negative departure of the *cmt* value from the corresponding ideal behavior indicates the fact that the mixed micellization is taking place at lower concentration. In other words such a situation can be explained on the basis of greater hydrophobicity attained by the mixed micelle which derives the mixed micellization at low concentration. Similar qualitative behavior has been observed from the variation of cmt_{exc} values.

From the variation of the plots of Fig. 2 one can therefore deduce that mainly strong interactions are present between the components of P103 + L64/P84 binary mixtures, while weak interactions are observed among rest of the binary mixtures.

Table 2
Values of *cmt* and cmt_{exc} (°C) of different triblock polymers at 5.0×10^{-4} mol dm^{-3} concentration

TBP	*cmt*	cmt_{exc}	Average	Literature values (conc.)
L64	41.0	41.0	41.0	39.5 [5] (3.45)[a]
P103	22.0	22.0	22.0	22.5 [5] (5.05)[a]
P84	34.0	32.1	33.0	33.5 [5] (5.95)[a]
P104	26.0	26.0	26.0	25.5 [5] (4.24)[a]

[a] Represents the corresponding concentration value ($\times 10^{-4}$ mol dm^{-3}) of each TBP.

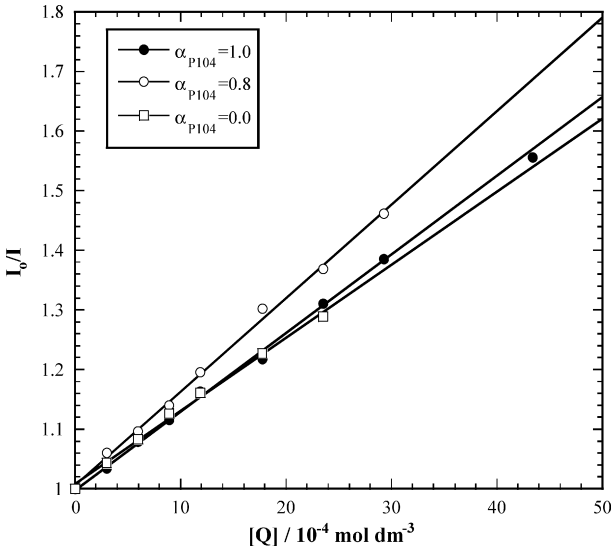

Fig. 3. Plot of I_0/I at the first vibronic band vs. [Q] for pure P104, P103 and $\alpha_{P104} = 0.8$ in P104 + P103 binary mixture at 45 °C.

3.1. Quenching process

The above results can further be explained on the basis of quenching of pyrene by a suitable quencher (Q) such as hexadecylpyridinium chloride (HPyCl) under steady state conditions. It is being assumed that the fluorescence lifetime of pyrene is longer than the residence time of the quencher in a micelle. A suitable [pyrene]/[mixed micelle] and [Q]/[mixed micelle] ratios ensure the Poisson distribution. The fluorescence intensity of the first vibronic band of pyrene decreases with the increase in [Q] without the appearance of any new band (not shown). A Stern–Volmer relationship can be used to explain the collision quenching under the steady state conditions [21–24]:

$$\frac{I_0}{I} = 1 + K_{SV}[Q] \quad (2)$$

where I_0 and I are the fluorescence intensities without and with quencher, respectively, and K_{SV} is the collisional quenching constant, called the Stern–Volmer constant. A linear variation of I_0/I versus [Q] (Fig. 3) will provide the value of K_{SV} for all pure and mixed components. These K_{SV} values thus obtained have been plotted in Fig. 4 for various binary mixtures.

Fig. 4 shows that K_{SV} value varies nonlinearly with positive deviations from the ideality, which are predominant in the

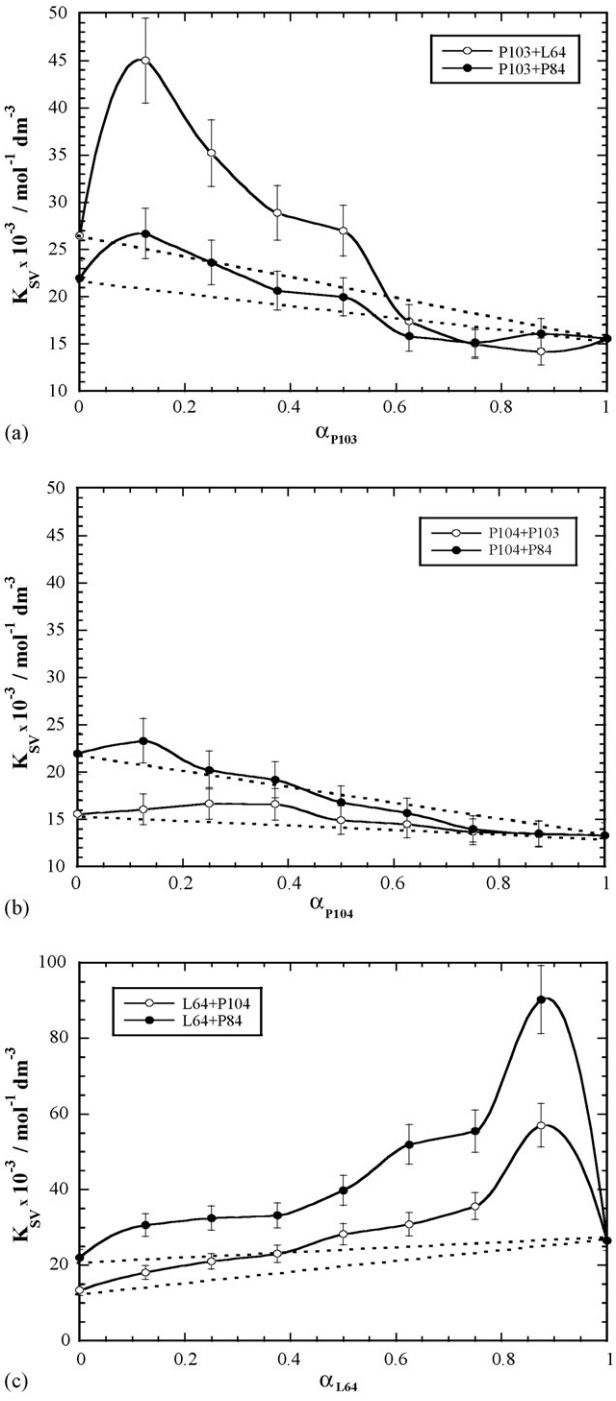

Fig. 4. Plot of K_{SV} vs. $\alpha_{P103/P104/L64}$: (a) P103 + L64/P84 binary mixtures, (b) P104 + P103/P84 binary mixtures and (c) L64 + P104/P84 binary mixtures.

case of P103 + L64/P84 thus demonstrating that the quenching is facilitated in these mixtures. This can be attributed to the presence of suitable hydrophobic environment provided by the mixed micelles for the favorable solublization of pyrene where effective quenching takes place. Thus, the origin of stronger interaction in P103 + L64/P84 in comparison to rest of the mixtures might be arising from a large difference in the *cmt* values of two components and could be responsible for the attractive interactions between the components in the mixed state. A close inspection of Fig. 2(a) and (b) indicates that binary mixtures of P103 + L64/P84 have large difference in the *cmt* values of the pure components which might generate a large unequal dehydration of the respective micelles under the effect of temperature variation. Such unequal dehydration may cause rearrangement of the triblock polymer monomers in the mixed state in such a way so that some of the ethylene oxide groups remain in contact with water, thus generating required stability while maintaining a stronger hydrophobic environment.

3.2. Kinetics of excimer formation

The excimer emission is produced by the collosional quenching between the excited (Py^*) and ground state (Py) monomers of the fluorescence probe. Thus, the mechanism of the excimer dimer (D^*) formation can be written in the following way:

$$Py^* + Py \underset{k_{ED}}{\overset{k_{EF}}{\rightleftharpoons}} D^* \tag{3}$$

$$Py^* \xrightarrow{k_{MF}} Py + h\nu \tag{4}$$

$$D^* \xrightarrow{k_{DF}} 2Py + h\nu \tag{5}$$

where k_{EF}, k_{ED}, k_{MF}, and k_{DF} are the constants of excimer formation, excimer dissociation, monomer fluorescence, and dimer fluorescence, respectively. Apart from this, there are other non-radioactive decays of Py^* and D^* which have been not shown here. The detailed analysis of this kinetic process has been reported by Briks et al. [25–27]. For simplification two sets of experimental conditions, i.e. low temperature and high temperature behaviors within the temperature range studied herein have been discussed. At low temperature I_{exc}/I_1 ratio can be written as

$$\frac{I_{exc}}{I_1} = \frac{k_{EF}^1[Py]}{k_{MF}} \exp\left[-\frac{W_{EF}}{kT}\right] \tag{6}$$

where k_{EF}^1 and W_{EF} are the frequency factor (limiting value of k_{EF} as $T \to \infty$) and activation energy of excimer formation,

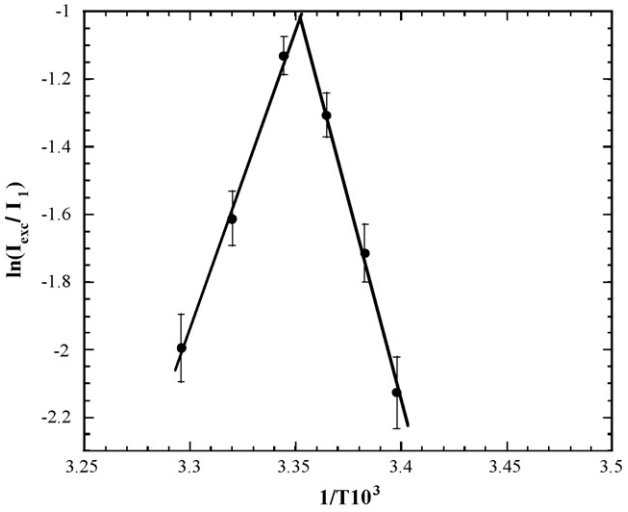

Fig. 5. Plot of $\ln(I_{exc}/I_1)$ vs. $1/T$ for pure P104 at [P104] = 5.0×10^{-4} mol dm^{-3}.

respectively, and k is Boltzmann's constant. Similarly, at high temperature, the I_{exc}/I_1 ratio is given by

$$\frac{I_{exc}}{I_1} = \frac{k_{DF}k^1_{EF}[Py]}{k^1_{ED}k_{MF}}\exp\left[\frac{B}{kT}\right] \quad (7)$$

where B is the excimer binding energy = $W_{ED} - W_{EF}$ and k^1_{EF} is the frequency factor. Eqs. (6) and (7) suggest that a plot of $\ln I_{exc}/I_1$ increases and decreases linearly with $1/T$, respectively, at fixed [Py]. Fig. 5 shows such a variation for P104 at different temperatures. Here too, an interaction of two linear lines gives the *cmt* equal to 26 °C. Hence, the kinetics of pyrene solubiliza-

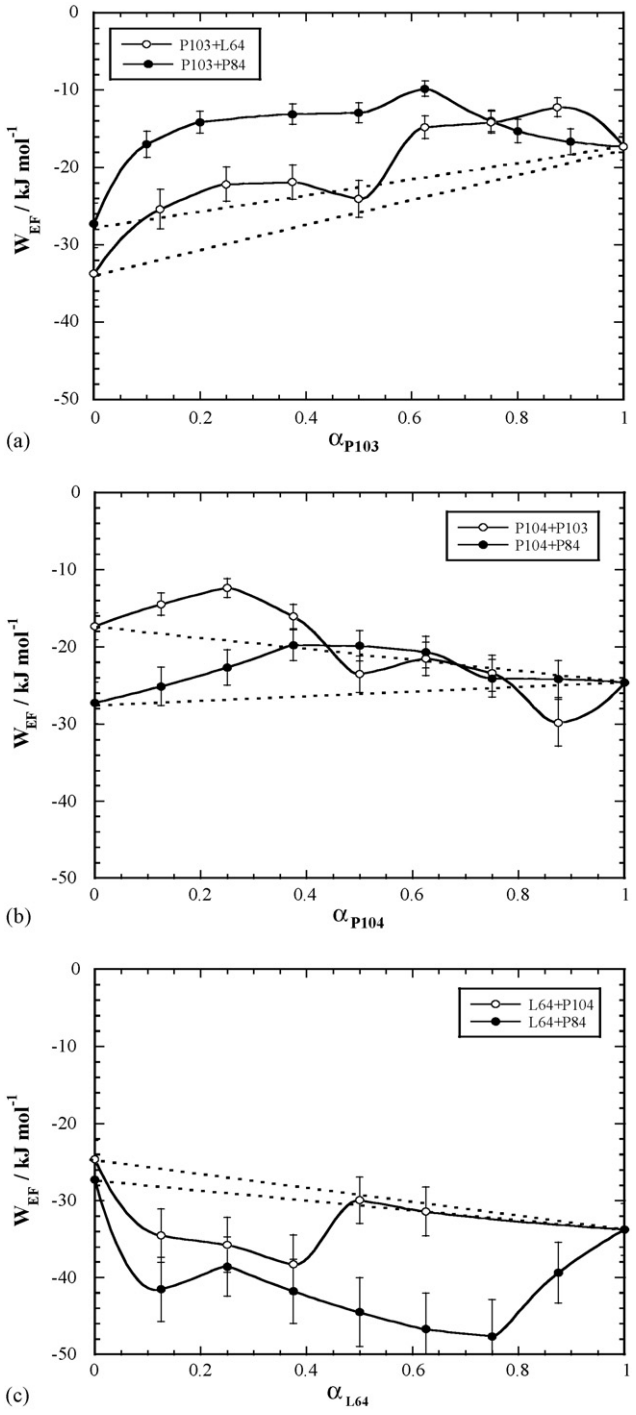

Fig. 6. Plot of energy of activation (W_{EF}) of the pyrene probe for the excimer formation vs. $\alpha_{P103/P104/L64}$ of (a) P103 + L64/P84 binary mixtures, (b) P104 + P103/P84 binary mixture and (c) L64 + P104/P84 binary mixtures.

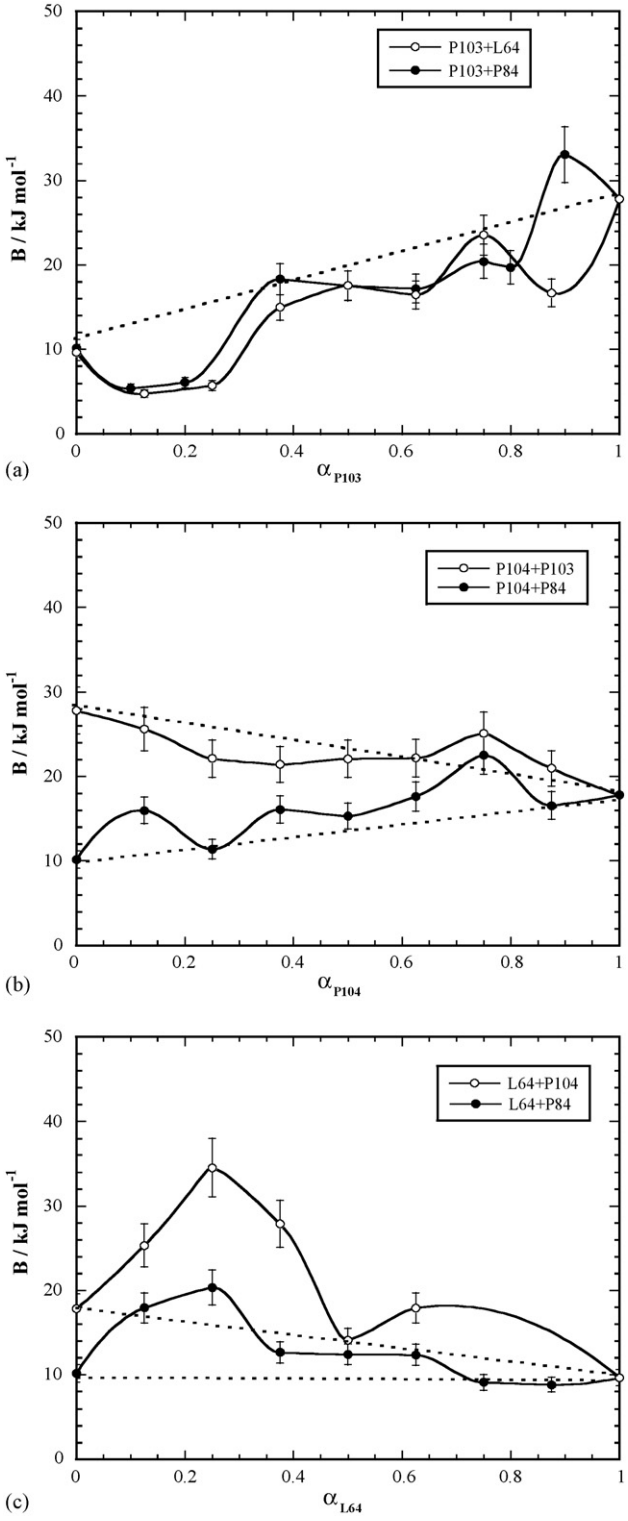

Fig. 7. Plot of binding energy (B) of the pyrene probe for the excimer formation vs. $\alpha_{P103/P104/L64}$ of (a) P103 + L64/P84 binary mixtures, (b) P104 + P103/P84 binary mixture and (c) L64 + P104/P84 binary mixtures.

tion in TBP micelles can be analysed within two different sets of experimental conditions, i.e. below and above 26 °C. The former gives the activation energy (W_{EF}) for excimer formation by pyrene while the latter gives the binding energy (B) of excimer formation. Both values thus obtained for various pure and mixed TBP mixtures have been plotted in Figs. 6 and 7.

Fig. 6 shows the variation of W_{EF} over the whole mole fraction range for all mixtures. These values for P103 + L64/P84 (Fig. 6(a)) show a positive deviation from the ideal mixing (shown by dotted lines), while those for P104 + P103/P84 (Fig. 6(b)) remain mostly close to ideal behavior. Fig. 6(c) shows negative deviations in W_{EF} values from ideality for L64 + P104/P84 mixtures. A decrease in the W_{EF} values at all mole fractions of P103 + L64/P84 in Fig. 6(c) can be attributed to the facilitation of the excimer formation which is also evident from the higher K_{SV} values (Fig. 4(a)) for these mixtures. These results can also be related to the relative viscosity (η_r) behavior for these mixtures (Fig. 8(a)). A smaller η_r value than ideal behavior especially in the P103 poor region of the mixtures show the attractive interactions between the components and that might be responsible for lower W_{EF} in comparison to their pure states. This is further supported by the negative deviations in B values from the ideal behavior (Fig. 7(a)). A closeness between the W_{EF} and corresponding ideal behavior (Fig. 6(b)) for P104 + P103/P84 mixtures further confirm the presence of predominantly ideal behavior. The variation in the B values for these mixtures (Fig. 7(b)) fully supports this fact. The η_r of P104 + P84 mixtures (Fig. 8(b)) shows clear ideal mixing but the negative deviation in the case of P104 + P103 is due to unknown reasons. An increase in the W_{EF} value for L64 + P103/P84 mixtures (Fig. 6(c)) from their pure components clearly indicates the reduction in excimer formation. This is again complimentary with the positive deviations in the B values from the corresponding ideal mixing (Fig. 7(c)). Both figures (i.e. Figs. 6(c) and 7(c)) demonstrate that the variation in W_{EF} and B values mainly predominant in the L64 poor regions of both mixtures. The positive deviation in the η_r (Fig. 8(c)) from ideal behavior especially in the L64 poor region further confirm these results.

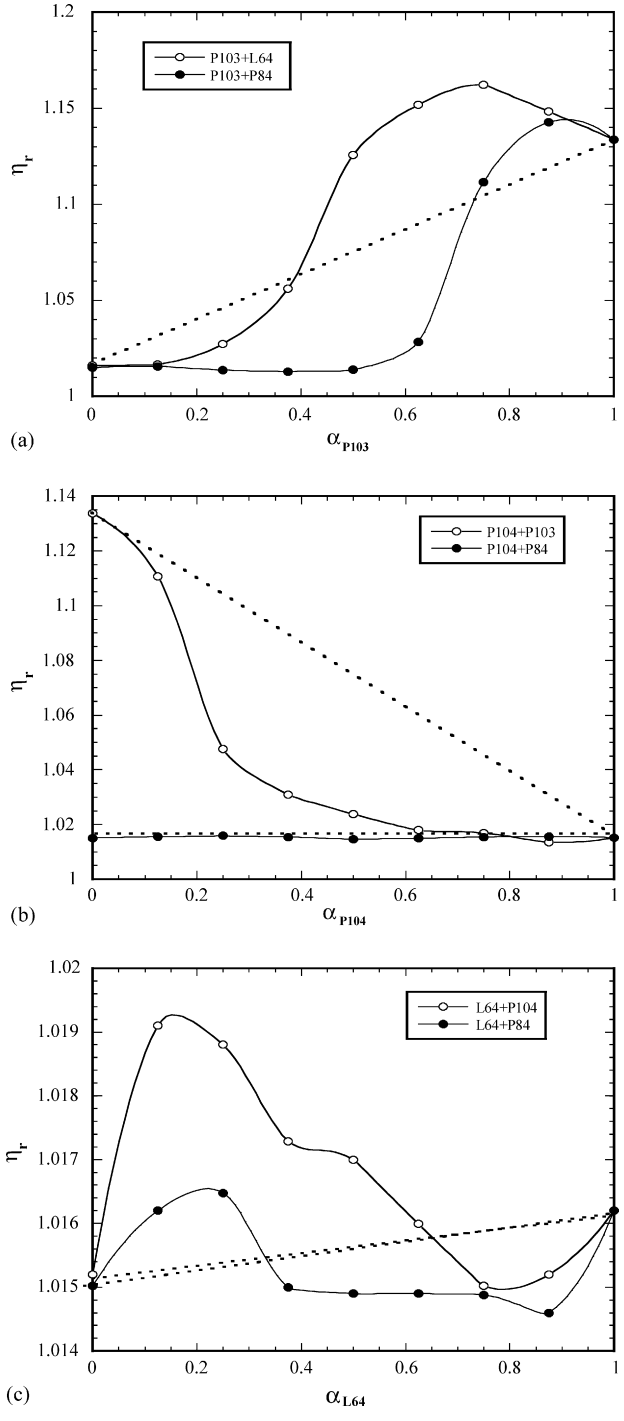

Fig. 8. Plot of η_r vs. $\alpha_{P103/P104/L64}$: (a) P103 + L64/P84 binary mixtures, (b) P104 + P103/P84 binary mixtures and (c) L64 + P104/P84 binary mixtures.

4. Conclusions

The variation of all micellar parameters and photophysical properties indicate that the mixed micelles between the components of P103 + L64 and P103 + P84 mixtures form due to attractive interactions. These interactions arise from the mutual compatible arrangement among the unlike TBP monomers in the mixed state in such a way so that steric hindrances are minimized. We believe that the large difference among the *cmt* values of individual components proves to be favorable for their stable mixed micelles.

On the other hand, mixtures of P104 + P103 and P104 + P84 prefer to remain ideal in their mixed state, while the mixtures of L64 + P104 and L64 + P84 show mainly unfavorable mixing.

Acknowledgement

Financial assistance to N. Kaur from University Grants Commission, New Delhi, is thankfully acknowledged.

References

[1] M. Almgren, W. Brown, S. Hvidt, Colloid Polym. Sci. 273 (1995) 2.
[2] I.R. Schmolka, J. Am. Oil Chem. Soc. 54 (1977) 110.
[3] P. Bahadur, G. Reiss, Tenside Surf. Deterg. 28 (1991) 173.
[4] B. Chu, Langmuir 11 (1995) 4142.
[5] P. Alexandridis, J.F. Holzwarth, T.A. Hatton, Macromolecules 27 (1994) 2414.

[6] P. Alexandridis, T.A. Hatton, Colloids Surf. A 96 (1995) 1.
[7] Pluronic and Tetronic Block Copolymer Surfactants, BASF Corp., 1989, Technical brochure.
[8] P. Alexandridis, J.F. Holzwarth, Curr. Opin. Colloid Interf. Sci. 5 (2000) 312.
[9] K. Mortensen, J.S. Pedersen, Macromolecules 26 (1993) 805.
[10] E. Hecht, H. Hoffmann, Colloids Surf. A 96 (1995) 181.
[11] I. Goldmints, G.E. Yu, C. booth, K.A. Smith, T.A. Hatton, Langmuir 15 (1999) 1651, and references therein.
[12] M.J. Kositza, C. Bohne, P. Alexandridis, T.A. Hatton, J.F. Holzwarth, Macromolecules 32 (1999) 5539.
[13] L. Yang, P. Alexandridis, D.C. Steytler, M.J. Kositza, J.F. Holzwarth, Langmuir 16 (2000) 8555.
[14] A. Genz, J.F. Holzwarth, J. Eur. Biophys. 13 (1986) 323.
[15] K. Kortensen, Europhys. Lett. 19 (1992) 599.
[16] M. Bohorque, C. Koch, T. Trygstad, N. Pandit, J. Colloid Interf. Sci. 216 (1999) 34.
[17] G. Wanka, H. Hoffmann, W. Ulbricht, Macromolecules 27 (1994) 4145.
[18] P. Linse, M. Malmsten, Macromolecules 25 (1992) 5434.
[19] P. Alexandridis, T. Nivaggioli, T.A. Hatton, Langmuir 11 (1995) 1468.
[20] M.S. Bakshi, P. Bhandari, S. Sachar, R.K. Mahajan, Colloids Polym. Sci. 284 (2006) 1363.
[21] O. Stern, M. Volmer, Phys. Z. 20 (1990) 18.
[22] A. Wellar, Prog. React. Kinet. 1 (1976) 3246.
[23] M.R. Efthik, C.A. Gheron, J. Phys. Chem. 80 (1976) 486.
[24] H. Gorner, C. Stammel, J. Mattey, J. Photochem. Photobiol. A: Chem. 120 (1997) 171.
[25] J.B. Briks, L.G. Christrophorou, Proc. Roy. Soc. Lond. Ser. A 274 (1963) 552.
[26] J.B. Briks, L.G. Christrophorou, Proc. Roy. Soc. Lond. Ser. A 277 (1964) 51.
[27] J.B. Briks, M.D. Lumb, I.H. Munro, Proc. Roy. Soc. Lond. Ser. A 280 (1963) 289.